Combust. Sci. and Tech., 1996, Vol. 120, pp. 55–81
Reprints available directly from the publisher
Photocopying permitted by license only

The Comparison of Two Comprehensive Combustion Codes to Simulate Large-Scale, Oil-Fired Boilers

C. F. M. COIMBRA[c], P. J. COELHO[b],
M. Q. McQUAY[a] and M. G. CARVALHO[b]

[a]*Brigham Young University, Department of Mechanical Engineering, 242-CB Provo, UT 84602 USA;* [b]*Instituto Superior Técnico, Departamento de Engenharia Mecânica, Av. Rovisco Pais, 1096 Lisboa CODEX, Portugal;* [c]*University of California at Irvine, Department of Mechanical and Aerospace Engineering, Irvine, CA 92717 USA*

(Received 29 September 1995; In final form 29 July 1996)

This article compares numerical predictions made by two independent comprehensive numerical codes for the radiant section of a 250 MWe, oil-fired boiler of the Setúbal Power Plant in Portugal. Local properties predicted by the two different models are also compared to experimental data obtained for the same boiler. The two numerical codes are finite-volume based, but they employ different mesh arrangements, optical properties, radiation, and oil vaporization submodels. In general, despite the different submodels used, both predictions were in good agreement. The predictions were also within engineering accuracy of the available experimental data. Detailed analysis of the predictions for the near burner region showed moderate differences in the results of the two models. This implies that, although of fundamental relevance for pollutant formation, the uncertainties on the prediction of the near-burner region do not affect significantly the predicted results far from the burners. This result is expected, since local equilibrium and chemical balance are achieved at the less reactive regions, such as the ones for which the predictions were compared to the available experimental data.

Keywords: Mathematical modelling; utility boilers; combustion in practical systems

1. INTRODUCTION

The energy industry is now facing a dramatic change in the designing tools normally used in the development of cleaner technologies for fossil fuel energy use. Essentially an academic exercise for modeling practical reactors

during the past decade, large-scale combustion modeling is now being used as a practical tool in the quest for more affordable, cleaner combustion furnaces. Comprehensive numerical codes have been developed to model oil, gas, and coal flames at various scales. This work compares the performance of two such comprehensive codes and their reliability in predicting local properties on industrial-scale, reactive flows. The two codes, the product of continuous research efforts performed at Brigham Young University (BYU) and Instituto Superior Técnico (IST), are designated in this paper as BYU-CODE and IST-CODE respectively.

Most of the recent developments in large-scale modeling were driven by current pollution regulations. Models to adequately describe reactive flows in industrial environments and to predict accurately species concentration distributions and pollutant formation are still being developed. Increased interest in this area can be measured by the ever-growing number of publications concerning experimental studies (see, e.g., Anson *et al.*, 1974; Barlow, 1982; Abraham and Rajaram, 1983; Bonin and Queiroz, 1991; Butler and Webb, 1991; Queiroz *et al.*, 1993; Cassiano *et al.*, 1994; Heitor *et al.*, 1994) and numerical studies on industrial-scale boilers (see, e.g., Xu, 1981; Shida *et al.*, 1982, Sakai *et al.*, 1982; Benesh and Kremer, 1984; Robinson, 1985; Boyd and Kent, 1986; Fiveland *et al.*, 1987; Truelove and Williams, 1988; Lockwood *et al.*, 1988; De Michelle *et al.*, 1989; Gillis and Smith, 1990; Carvalho and Coelho, 1990; Chen *et al.*, 1992; Aoki *et al.*, 1992; Coelho and Carvalho, 1993; Coimbra *et al.*, 1994; Mann and Kent, 1994; Gopinath and Ganesan, 1994; and Carvalho *et al.*, 1994). Also interesting is the fact that these and other relevant publications represent the efforts of many different research institutions from several countries. The globalization of the research on fossil fuel utilization reflects the importance of this subject for the development of a better and cleaner global environment.

Several comprehensive numerical codes have been used to simulate combustion in industrial equipment, but because very little experimental data is available for these large-scale facilities, the validation of the submodels employed is generally limited, as is the general reliability of the codes used. Lately, more detailed experimental data became available in the literature, allowing a more extensive validation of the applications of the numerical submodels to large-scale boilers. These submodels include model descriptions of the processes of radiation, gas combustion, droplet or particle reaction, and gas and particle aerodynamics. Without exception, all these submodels were developed with the aid of lab-scale facilities (see, e.g., Lockwood *et al.*, 1980; Smoot, 1981; Truelove, 1986; Rizvi, 1985; Costa *et al.*, 1990; Hanjalic and Sijercic, 1994; Sijercic and Hanjalic, 1994). Although

extensively validated at the laboratory scale, evaluation of these submodels in full-scale equipment presents additional challenges. For example, the role of radiation transport becomes more important as the overall dimensions of the furnace increase. Hence, the application of the numerical submodels to large-scale simulation is not straightforward, and needs support from experiments performed at full-scale, boiler-operating conditions. This paper provides the first comparison of the predictive capabilities of two comprehensive numerical codes with in-situ experimental data taken for a full-load, normal operating condition of a 250 MWe, oil-fired, industrial-scale boiler.

A brief description of the main features of the two codes is given in the next section. Then, the simulated boiler is described and the results are presented and discussed. The main conclusions are drawn in the last section.

2. SUMMARY OF THE COMPREHENSIVE CODES

As mentioned earlier, both numerical codes are finite-volume based. The procedure for the solution of the gas flow field consists on the discretization and solution of the general transport equation (Equation 1). This equation is solved in a steady-state, Favre-averaged fashion for all primitive variables (u_i, p, h) of the flow field, and all combustion (f_k, g_k) and turbulence quantities (k, ε).

$$\frac{\partial}{\partial x_i}(\rho_g u_{i;g} \phi) = \frac{\partial}{\partial x_i}\left(\Gamma_\phi \frac{\partial \phi}{\partial x_i}\right) + S_g + S_d \tag{1}$$

ϕ in this equation stands for the transported property, and S is a source term originated either from the gas or the dispersed phase (subscripts 'g' or 'd'). Γ_ϕ is the diffusion coefficient for the property ϕ. The subscript 'k' in the combustion variables 'f' and 'g' (mixture fraction and its variance) refers to the use of more than one mixture fraction, a feature that was included in the BYU-CODE to allow for the calculation of steam-atomized sprays. Although this second mixture fraction and its variance (f_2, g_2) for the steam were not used in the simulations presented in this paper, some preliminary simulations of a corner-fired, utility boiler made use of these variables (Coimbra and Queiroz, 1994).

The governing equations are integrated over each control volume and discretized using finite differences. The central difference scheme is employed for all but the convective terms which are discretized using the hybrid

central difference/upwind scheme. The solution algorithm is based on the SIMPLE method. The algebraic sets of discretized equations are solved using the Gauss-Seidel line-be-line iteration procedure.

2.1. The BYU Code

The oil-combustion model developed at Brigham Young University was implemented in the PCGC-3 platform (Pulverized Coal Gasification and Combustion -- Three-Dimensional). This code has been developed during the past ten years by BYU researchers to simulate various combustion-related equipment (see, e.g., Hill and Smoot, 1993). The original platform of the code consists of a staggered, orthogonal arrangement of finite-volume numerical cells to solve the discretized, time-averaged, Navier-Stokes equations. Turbulence is handled by either the standard eddy-viscosity or by the nonlinear k-ε models. The simulations performed for this paper used the standard k-ε model.

Combustion is modeled assuming local equilibrium chemistry through the use of a subroutine designed to create an equilibrium look-up table. This subroutine calculates the equilibrium solution through the construction of an auxiliary Newton-Raphson derivative matrix for the equilibrium solution and solves it using pivotal Gaussian reduction. A mixture fraction is defined as the conserved scalar to be transported in order to reduce the calculation effort of solving one transport equation for each species of interest. The use of the mixture fraction is also reinforced by the fact that, for most of the chemical reactions, the turbulence mixing is dominant to the chemical kinetics. In fact, only the chemical reactions for CO and NO_X present time scales of the order of the turbulence time scales. The species considered for the formation of the look-up table in this paper were O_2, CO_2, H_2O, CH_4, C (solid), CO, SO_2 and the fuel oil, which has its composition given in terms of C, H, N, S, and H_2O.

Radiation in the BYU-CODE is handled by the Discrete-Ordinates method (see, e.g., Fiveland, 1987). A spectral method is used for the derivation of the optical properties of the gas phase. This method employs a weighted sum of grey gases and avoids the estimation of a characteristic optical thickness of the medium. The advantage of this method is the fact that the optical thickness is calculated instead of being estimated as a global parameter (Denison and Webb, 1993).

The oil-droplet trajectories are calculated in the Lagrangian framework through a stochastic solution of the momentum equation for the droplets. The initial conditions and the starting locations for each stream of droplets

in each burner were estimated based on the characteristics of spray atomizers similar to the ones used in the Setúbal Power Plant boilers. The droplet sizes were discretized in ten different diameters following a Rosin-Ramler distribution with mean value of 55 microns. Parametric calculations showed that for the level of grid refinement used here the determination of the exact initial conditions of the spray is not crucial to the quality of the results. Equation 2 is the droplet momentum equation adopted for this work.

$$m_d \frac{\partial u_{i;d}}{\partial t} = 3\pi C_D \mu_g D_d + m_d g_i \tag{2}$$

In Equation 2, u_i is the instantaneous cartesian velocity in the i-direction, μ_g is the laminar viscosity of the gas, D_d is the droplet diameter, and C_D is the Reynolds-Prandtl-dependent drag coefficient for a sphere. g_i is the component of the gravity acceleration in the i-direction. Buoyancy is considered in the momentum equation for the droplets, but neglected in the corresponding equation for the gas. Equation 2 can be rewritten in terms of the particle relaxation time τ, leading to the following expression

$$\frac{du_{i;d}}{dt} = \frac{1}{\tau}(u_{i;g} - u_{i;d}) + g_i, \tag{3}$$

where τ is defined as

$$\tau = \frac{24\rho_d \mathrm{D}_d^2}{18\mu_g C_D \mathrm{Re}_d}, \tag{4}$$

and where ρ_d is the specific mass of the droplet. The droplet Reynolds number Re_d is defined as

$$\mathrm{Re}_d = \frac{\rho_g \mathrm{D}_d |\vec{V}_d - \vec{V}_g|}{\mu_g}. \tag{5}$$

Equation 3 is a first-order, nonhomogeneous, nonlinear, differential equation which can be integrated analytically if very small time steps are considered. The integration of Eq. 3 gives the droplet velocity at each time step. The components of this velocity are used to determine the next position of the droplet in the trajectory as follows:

$$u_{i;d}{}^{i+1} = u_{i;g} + \tau g_i + (u_{i;d}{}^{i} - u_{i;g} - \tau g_i) e^{-\Delta t/\tau} \tag{6}$$

The addition of a turbulent, droplet-dispersion model (which makes the solution procedure stochastic) must be carefully implemented to avoid prohibitive numerical costs. The general procedure to implement a Stochastic-Separated-Flow (SSF) model in a tracking routine for a n-dimensional flow field is as follows: (1) estimate the starting location and the initial velocity for a droplet with a given initial size; (2) determine n-components of the gas velocity for this location; (3) based on the local turbulent quantities for the gas phase and the variance of the velocity of the gas, calculate n-random fluctuating velocities from a predetermined PDF for the fluctuations; (4) add the local fluctuating velocity components to the local gas velocity components and solve Equation 6 to determine the next droplet velocity; (5) integrate the velocity equation over the time step given by the minimum of the local eddy crosstime and the local eddy lifetime to determine a new droplet position (see, e.g., Truelove, 1986); (6) determine the new position of the droplet, the mass, the momentum, and the energy transfer during the time step, using interpolated properties from the old and the new positions; (7) using the new position, go back to step (2) and perform the steps (2) to (7) until the droplets react completely.

Heat and mass transfer are considered for the oil droplets through a two-stage process: preheating to the boiling temperature with no mass transfer and then heat-transfer-controlled vaporization at constant temperature (see Barreiros *et al.*, 1993). The energy equation for the droplets is integrated analytically to give the following rates of change for temperature (first stage) and diameter (second stage)

$$T_d^{i+1} = T_g + (T_d^i - T_g)\exp\left(-\frac{6k_g\,\mathrm{Nu}}{\rho_d\,\mathrm{C}_{P_d}\,\mathrm{D}_d^2}\Delta\mathrm{t}\right) \tag{7}$$

$$D_d^{i+1} = \left((D_d^i)^2 - C\frac{8k_g\ln(1+B)}{\rho_d\,C_{P_d}}\Delta t\right)^{1/2} \tag{8}$$

were C is an empirical convection factor and B is the transfer number defined below:

$$C = 1 + \frac{0.278\,\mathrm{Re}_d^{1/2}\,\mathrm{Pr}^{1/3}}{\left[1 + \dfrac{1.237}{\mathrm{Re}_d\,\mathrm{Pr}^{4/3}}\right]^{1/2}} \tag{9}$$

$$B = \frac{Cp_g(T_g - T_d)}{L} \tag{10}$$

In the above equations, L stands for the latent heat of vaporization and C_p and k are the specific heat capacity and conductivity, respectively. The Nusselt number for the droplets is defined in Equation 11:

$$\mathrm{Nu} = 2.0 + 0.55\,\mathrm{Re}_d^{1/2}\,\mathrm{Pr}^{1/3} \tag{11}$$

The source terms calculated by the Lagrangian subroutine are then added to the gas flow field through the respective droplet source term in Eq. 1. To allow for a better coupling between the terms generated by the stochastic Lagrangian procedure and the time-averaged, continuous flow field, a variable under-relaxation technique for the droplet source terms was used (see, e.g., Coimbra *et al.*, 1994). The droplet reaction model is described in detail in Barreiros *et al.* (1993).

2.2. The IST Code

As in the BYU-CODE, the combustion model in the IST-CODE is based on the assumptions that the reaction rates are very fast compared to the turbulence mixing rates, and that the mass diffusion and thermal diffusion coefficients are equal. Hence, combustion is described by means of a conserved scalar/prescribed PDF approach. The instantaneous thermochemical state of the mixture is calculated assuming chemical equilibrium. The turbulence model used by the IST-CODE to perform the simulations presented here was also the standard k-ε model. Buoyancy is neglected in the momentum equations.

Radiation in the IST-CODE is handled by the Discrete Transfer Model (Lockwood and Shah, 1980), with optical properties for the gaseous mixture calculated by the use of a two-grey-and-a-clear-gas approach, extended to account for soot (Truelove, 1976). A transport equation for soot mass fraction was solved to calculate the distribution of soot concentration, which is required to determine the soot absorption coefficient. The soot formation model of Khan and Greeves (1974) and the soot oxidation model of Magnussen and Hjertager (1977) were used to compute the source term of the transport equation.

The droplet vaporization in the IST-CODE is considered to be instantaneous, and no exchange of heat and momentum is considered. The oil phase is treated as a gas with the same chemical composition of the oil, the liquid heat of vaporization being neglected, and the boundary conditions for the mixture fraction are adjusted to consider the fuel stream. This simplification, called the zero-way coupling between the phases, is acceptable if

the vaporization of the oil droplets occurs in a very short period of time (between 2 to 40 ms).

In the IST-CODE, Eq. 1 is also solved in an orthogonal, staggered mesh arrangement, but using a domain decomposition technique. The significant advantage obtained by domain decomposition techniques is the division of a large domain into smaller subdomains having independent and different grid refinements. The zonal method used in the IST-CODE allows the use of refined meshes close to regions of greater interest, and the use of coarser grids for the less reactive or less complex zones of the reactor. The use of this technique is particularly recommended for turbulent flows in which geometrical length scales with different orders of magnitude are present, such as in a full-scale boiler.

The solution of the governing equations for each zone requires previous knowledge of the fluxes across the overlapping regions of the zone considered. The treatment of the interblock boundaries ensures continuity of the dependent variables and flux conservation across the interfaces. The global fluxes conservation is satisfied by requiring that

$$\sum_i \sum_j F_{i,j}^{(c)} = \sum_l \sum_m F_{l,m}^{(f)} \tag{12}$$

where the indices extend over all the control volumes of the coarse zone (c) and the fine zone (f) in the overlapping region between the two zones. An integration procedure is used to transfer data from one zone to the other, and an interpolation method is employed to transfer data reversely. Details of the implementation of the zonal method used for the simulations presented here can be found in Coelho and Carvalho (1993).

Table I summarizes the differences in the submodels and numerical methods used in both numerical codes. It shows that the two numerical codes employed fairly different submodels to describe the same mechanisms of transport.

The boundary conditions are the same for the two codes. The laws of the wall are used in the momentum, turbulent quantities and energy equations, and the temperature of the walls is prescribed. At the exit plane, a zero gradient normal to the boundary is assumed for the dependent variables. The vertical velocity component is then corrected to ensure mass conservation.

3. THE BOILER UNDER STUDY

The furnace modeled in this paper is a front-wall-fired, oil-fueled, 250 MWe, industrial boiler. Simulation results for this boiler obtained using the IST code

TABLE I Numerical techniques used by the BYU and the IST codes

Submodel	*BYU*	*IST*
Turbulence	Standard k-ε	Standard k-ε
Gas Combustion	Look-Up Table Chemical Equilibrium	Look-Up Table Chemical Equilibrium
Radiation	Discrete Ordinates	Discrete Transfer
Optical Properties	Weighted Sum of Grey Gases Spectral Derivation of the Optical Properties	Two-Grey-and-a-Clear-Gas Approach Global Geometrical Parameter to Estimate Optical Thickness
Droplet Mechanics	Stochastic Trajectories	Instantaneous Vaporization (no droplets)
Droplet	Two-Step Life	Not Considered
Vaporization	D^2-law, Infinite Conduction	
Soot Formation	Not Considered	Model of Khan and Greeves (1974)
Soot Oxidation	Not Considered	Model of Magnussen and Hjertager (1977)
Solution of the Transport Equations	Finite-Volumes, Staggered Grids, No Local Refinement	Finite-Volumes, Staggered Grids, Local Refinement (Zonal method)

have been presented elsewhere (Carvalho *et al.*, 1994, Coelho and Carvalho, 1993). Here, emphasis is placed on the comparison between the results of the IST- and BYU-codes. The simulations were performed for the radiant section of the boiler, which is schematically depicted in Figure 1. This figure also shows the location of the six burners and the position of two of the inspection ports through which measurements were taken. The firing system consists of twelve burners arranged in three lines of four equally spaced atomizers and air suppliers. The combustion air entering through the three burners of a column rotates in the same direction. Burners in adjacent columns swirl in opposite directions. Therefore, there is a symmetry plane at $y = y_{max}/2$. The air-flow rate for full-load operating condition is 825 ton/h. Because the simulations assumed a plane of symmetry in the center of the boiler, only one half of the physical domain was considered.

Swirl was considered by estimating tangential velocities for both primary and secondary air flows. Based on the angle of the swirling vanes, the absolute values of these velocities were estimated to be 16.4 m/s for the primary air and 25.4 m/s

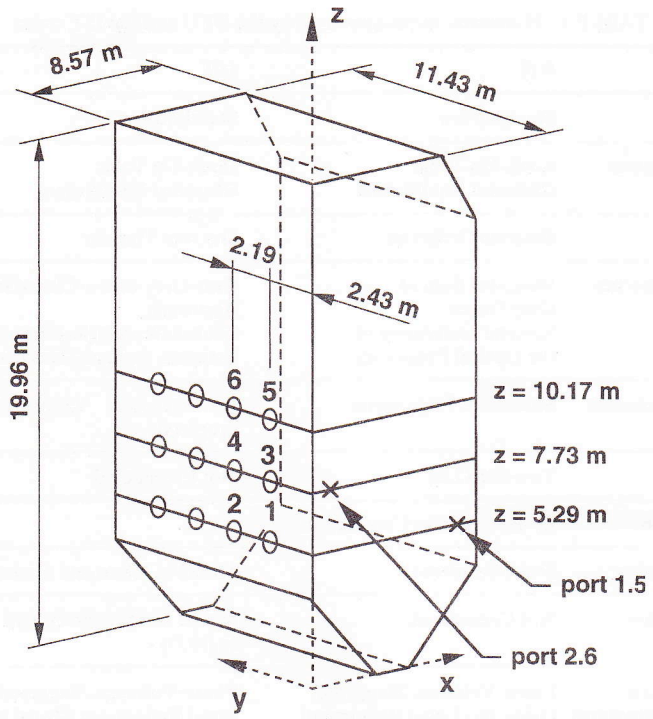

FIGURE 1 Sketch of the radiant section of the boiler.

for the secondary air. The ultimate analysis of the fuel used in both the BYU and IST simulations is shown on a mass basis in Table II.

In the simulations performed by the BYU-CODE, a grid arrangement of $50 \times 50 \times 100$ numerical cells was employed, with 100 nodes per burner. For the IST-CODE, three different regions were considered. The burner region was discretized using a $32 \times 41 \times 44$ mesh size, with 121 nodes per burner. The ash hopper employed $10 \times 18 \times 6$ grid nodes, and the top

TABLE II Residual fuel oil analysis used in the BYU and IST simulations

Carbon	86.52%
Hydrogen	11.06%
Nitrogen	0.72%
Sulphur	2.08% (ASTM D129)
Moisture	0.30% (vol.) (NP 1588)
Ash	0.07% (NP 1671)

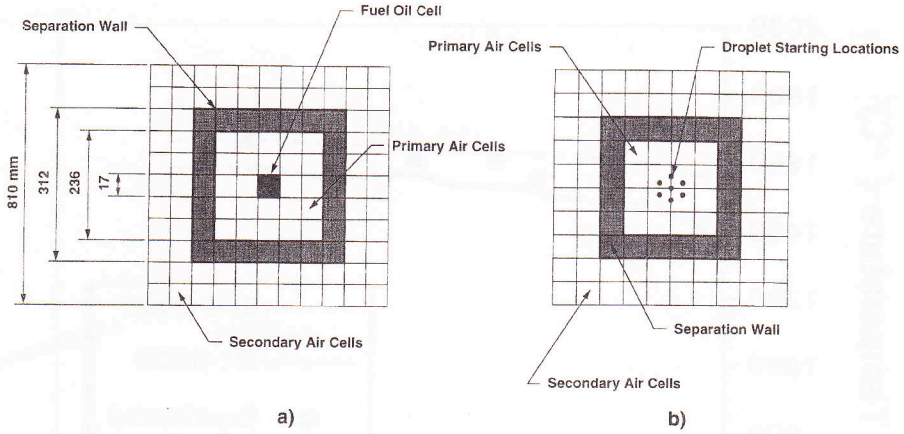

FIGURE 2 Discretization of the burners, a) IST-CODE b) BYU-CODE.

region of the boiler employed $16 \times 18 \times 8$ grid nodes. Details of the implementation of these zonal meshes can be found elsewhere (Carvalho *et al.*, 1994; Coelho and Carvalho, 1993). The discretization of the burners used in both codes is shown in Figure 2. A detailed description of the operating conditions and the experimental techniques used to characterize this boiler can be found in Cassiano *et al.* (1994).

A major difficulty in measuring local properties in industrial boilers is the limited access for the experimental probes. This is because industrial boilers were not designed to allow such measurements, and very few openings are available. In the case of the boiler modeled in this work, the experimental probes were inserted through the available inspection ports in the radiant section of the boiler (Cassiano *et al.*, 1994). Two sets of experimental data were used to compare the prediction capability of the two different codes. These data refer to temperature and species concentration (O_2, CO, and CO_2) profiles collected at two different ports in the boiler. These ports are referred in Cassiano *et al.* (1994) and Carvalho *et al.* (1994) as ports 1.5 and 2.6, and their coordinates in the frame of reference shown in Figure 1 are the following: port 1.5, $x = 8.12$ m, $z = 5.29$ m; port 2.6, $x = 0.45$ m, $z = 7.73$ m.

4. RESULTS AND DISCUSSION

Figure 3 shows the measured and calculated values of temperature for port 1.5. The experimental probe was inserted parallel to the rear wall at a

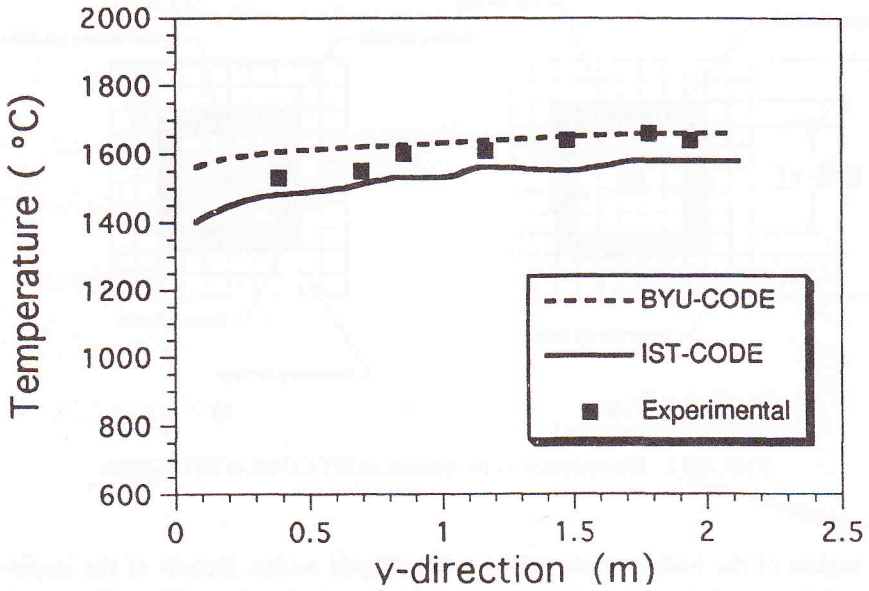

FIGURE 3 Comparison of predicted and measured temperatures through port 1.5.

distance of 0.45 m from that wall, and at the same level of the lowest row of burners. Experimental data were taken for values of y varying from the side wall to roughly 2.0 m of penetration. The dashed and the continuous line represent the results from the BYU-CODE and from the IST-CODE, respectively. As shown in this figure, the BYU-CODE slightly overpredicts the temperature, and the IST-CODE slightly underpredicts the temperature when compared to the experimental values for this port. However, both predictions are within the experimental uncertainty of the measured values ($\pm$ 50 K), demonstrating that both codes can predict temperature levels and trends in this region, far from the near-burner zone.

In general, the temperatures predicted by the BYU-CODE are slightly higher than the temperatures predicted by the IST-CODE, especially for the ash-hopper region and the region just above the burners (close to the radiant superheater). This trend can also be observed in Figure 4, which refers to the port 2.6, corresponding to the location of the intermediate row of burners. Because this port is close to the front wall, the experimental values taken for larger values of y were able to show the influence of the secondary air. This influence is shown in Figure 4 for values of y higher than 1.8 m. The temperature level is overpredicted by almost 100°C in the BYU-CODE simulation for values of y less than 1.8 m, but the trend of the

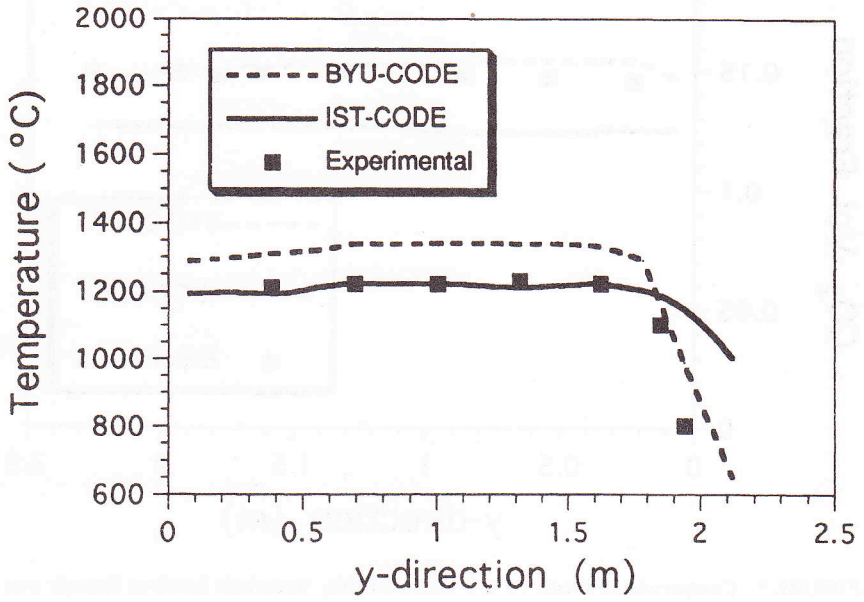

FIGURE 4 Comparison of predicted and measured temperatures through port 2.6.

temperature variation caused by the influence of the secondary air is very close to the experimental values. In the case of the IST-CODE, the temperature levels are perfectly predicted, but the impact of the cold air from the secondary stream is underestimated. Both codes were able to predict the correct trend of temperature variation of roughly 300°C from the front wall to the rear wall at the burner levels.

Figure 5 shows the measured and predicted values of CO_2 volumetric fraction for the same port as in Figure 3. The predictions shown in this figure indicate that the BYU-CODE predicts higher CO_2 volumetric fractions than the IST-CODE. Therefore, the higher temperature levels predicted by the BYU-CODE in the rear-wall region (see Fig. 3) are the result of a higher degree of mixing when compared to the IST-CODE. This is corroborated by Figure 6, which shows that the CO volumetric fraction, although being overpredicted in both simulations, is higher in the IST-CODE. In this region, the higher values of CO_2 predicted by the BYU-CODE also result from the convective effect of recirculating gases from the ash-hopper. As mentioned above, the ash-hopper temperature level is higher in the BYU-CODE simulation, indicating a more reactive ambient in this region, which favours the conversion of CO to CO_2. Both codes predict well O_2 concentrations in this region.

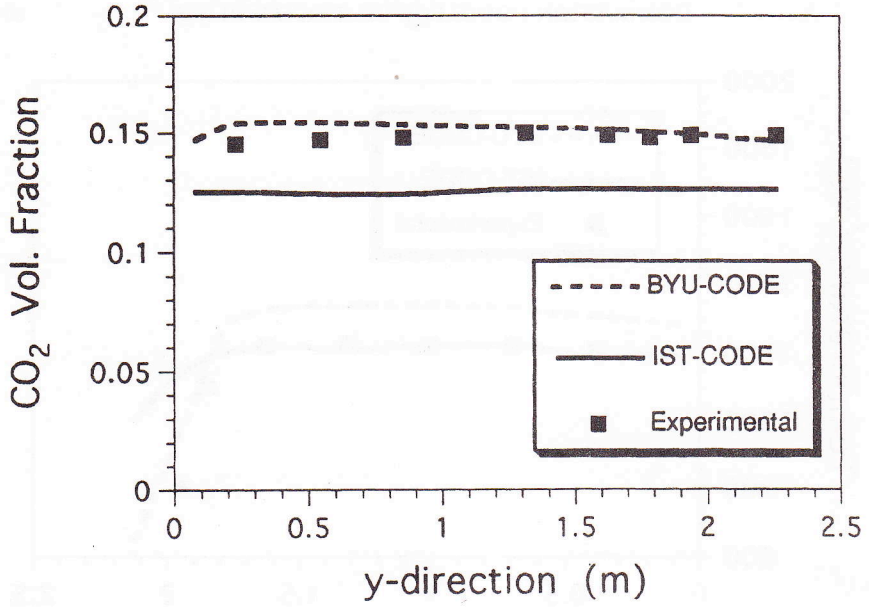

FIGURE 5 Comparison of predicted and measured CO_2 volumetric fractions through port 1.5.

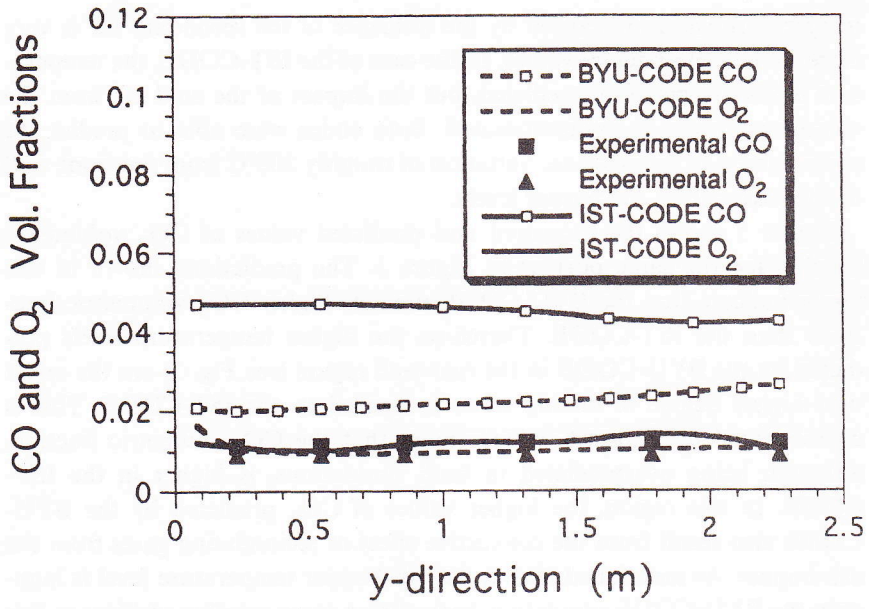

FIGURE 6 Comparison of predicted and measured CO and O_2 volumetric fractions through port 1.5.

Figure 7 shows the CO_2 volumetric fraction for the port 2.6, close to the front wall. Again, the relationship between Figure 7 and Figure 4 is evident. The lower values of CO_2 predicted by the IST-CODE are also associated with lower turbulence intensity levels in this region. Figure 8 shows that the CO volumetric fraction is overpredicted by both simulations, but more markedly by the IST-CODE. Oxygen concentrations are underpredicted by the BYU-CODE in this figure, but the steep gradient of O_2 concentrations caused by the cold air from the secondary stream is well predicted by both codes. The underprediction of O_2 by the BYU simulation is a result of the vaporization of the droplets, which cause steeper gradients in velocity, through the momentum source terms, with associated higher turbulence mixing. The higher micromixing levels enhance the depletion of the oxygen stream. It should be noticed that the near-burner region presents very complex flow patterns, and that, even with the most sophisticated kinetically controlled combustion models currently available, the prediction of this region would never be completely satisfactory with the use of eddy-viscosity turbulence models.

In general, and for the regions analyzed until now, both numerical codes agree quite well with each other and with the experimental data. Given the

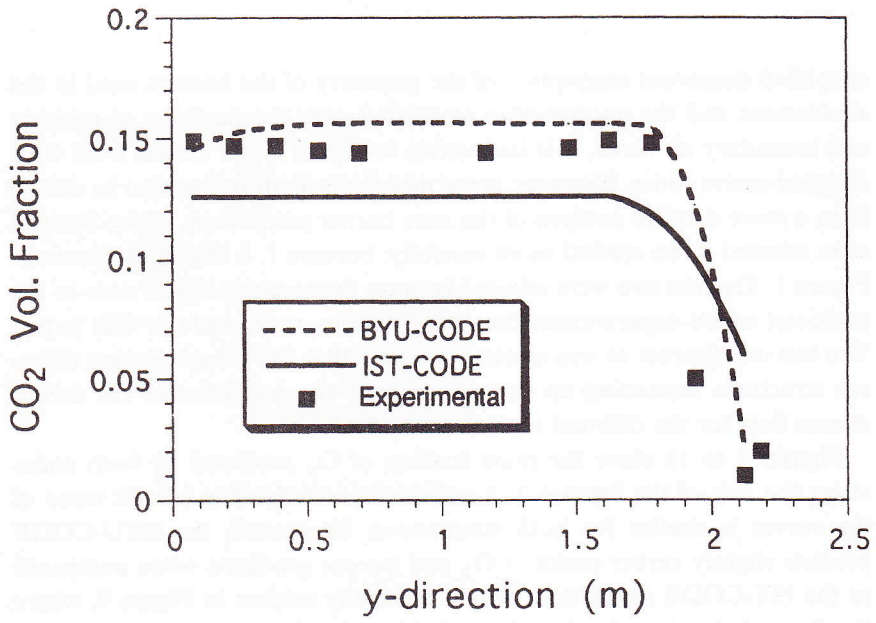

FIGURE 7 Comparison of predicted and measured CO_2 volumetric fractions through port 2.6.

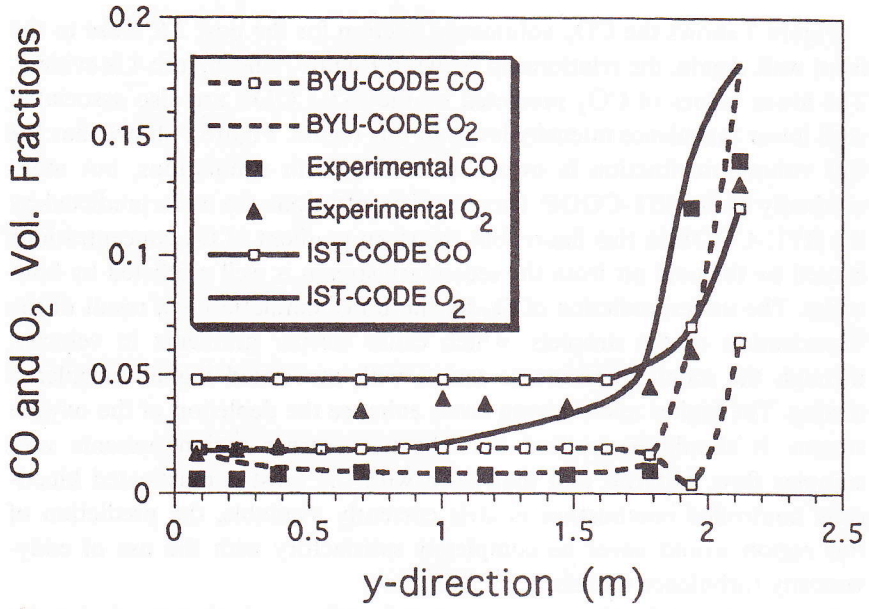

FIGURE 8 Comparison of predicted and measured CO and O_2 volumetric fractions through port 2.6.

simplified numerical description of the geometry of the burners used in the simulations and the uncertainties associated with the partition of primary and secondary air flows, it is impossible to expect better results from such comprehensive codes. However, some useful information can also be drawn from a more detailed analysis of the near burner predictions. Three burners were selected to be studied more carefully: burners 1, 3 and 6, as shown in Figure 1. The first two were selected because they are the closest ones to the positions where experimental data comparisons were made in this paper. The last one (burner 6) was selected to show that the flames present different structures depending on the aerothermal characteristics of the downstream flow for the different regions of the boiler.

Figures 9 to 11 show the mass fraction of O_2 predicted by both codes along the axis of the burners 1, 3 and 6, respectively. The overall trend of the curves is similar for both simulations. In general, the BYU-CODE predicts slightly earlier peaks of O_2 and steeper gradients when compared to the IST-CODE simulation. This is especially evident in Figure 9, where the flame feels strongly the effect of the recirculation in the ash-hopper region. For values of x greater than 3 m, the entrainment of the hot gases

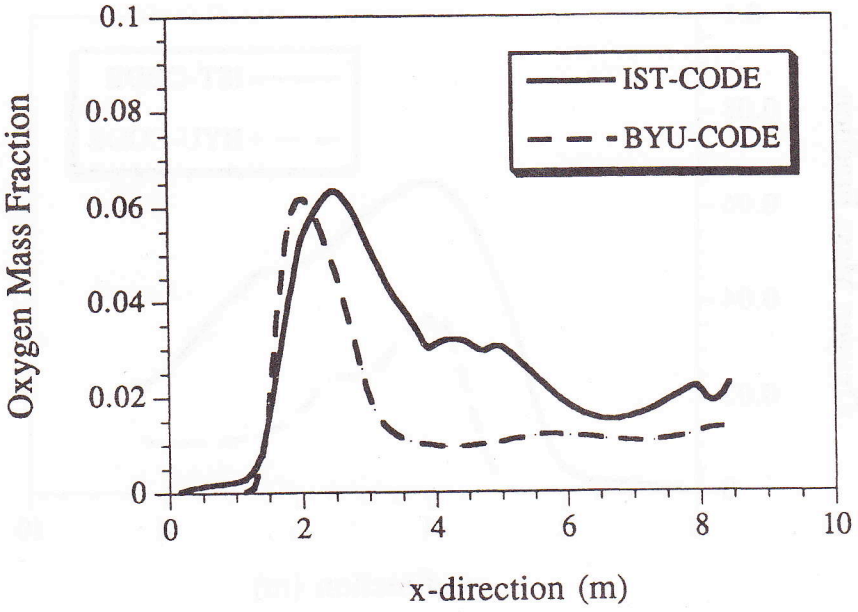

FIGURE 9 Predicted oxygen mass fractions along the axis of burner 1.

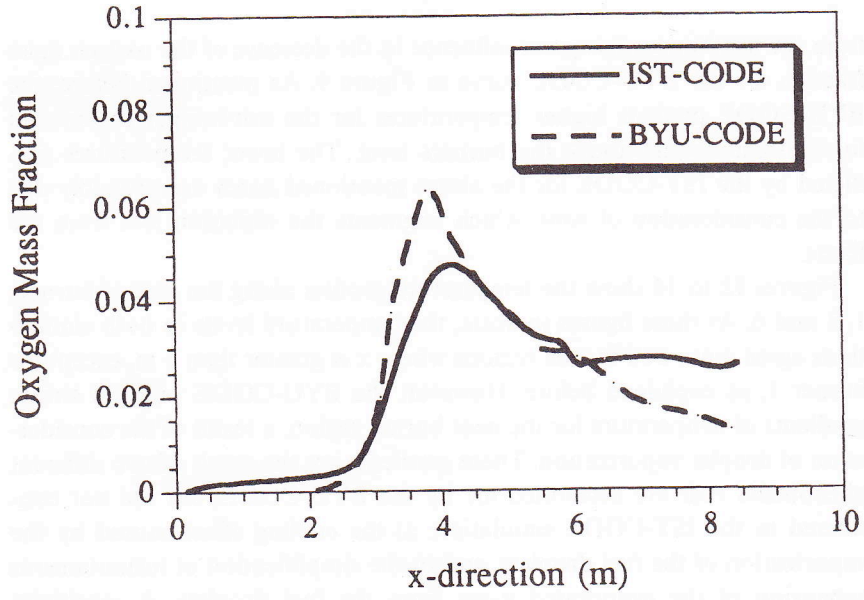

FIGURE 10 Predicted oxygen mass fractions along the axis of burner 3.

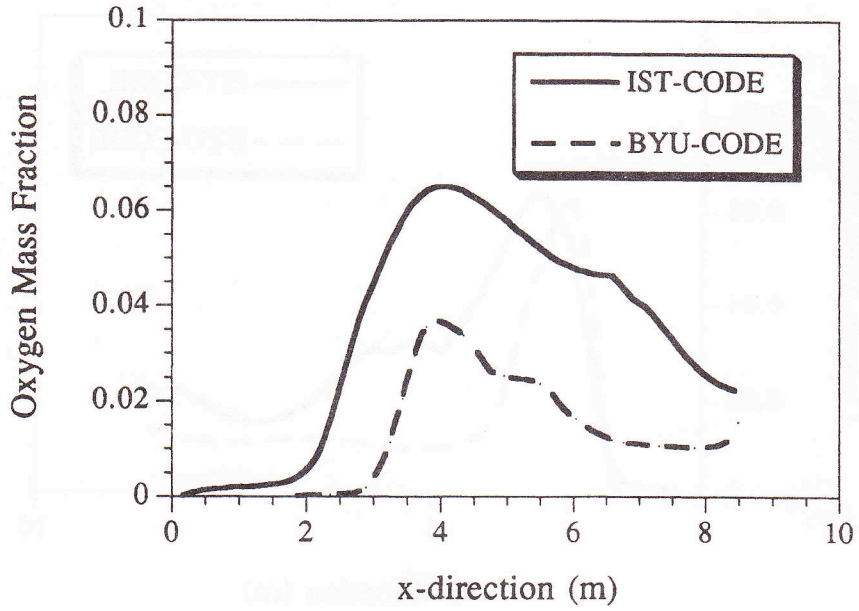

FIGURE 11 Predicted oxygen mass fractions along the axis of burner 6.

from the ash hopper has great influence in the decrease of the oxygen mass fraction for the BYU-CODE curve in Figure 9. As mentioned before, the BYU-CODE predicts higher temperatures for the ash-hopper region and for the regions just above the burners level. The lower temperatures predicted by the IST-CODE for the above mentioned zones are probably due to the consideration of soot, which augments the radiation loss from the flame.

Figures 12 to 14 show the temperature profiles along the axis of burners 1, 3 and 6. As these figures indicate, the temperature levels in both simulations agree quite well for the regions where x is greater than 3 m, except for burner 1, as explained before. However, the BYU-CODE predicts strong gradients of temperature for the near burner region, a result of the consideration of droplet vaporization. These gradients are the result of two different phenomena that are accounted for by the BYU-CODE, but are not considered in the IST-CODE simulation: a) the cooling effect caused by the vaporization of the fuel droplets, and b) the simplification of instantaneous expansion of the evaporated gases from the fuel droplets. A sensitivity analysis of the spray equations shows that the vaporization rate is very

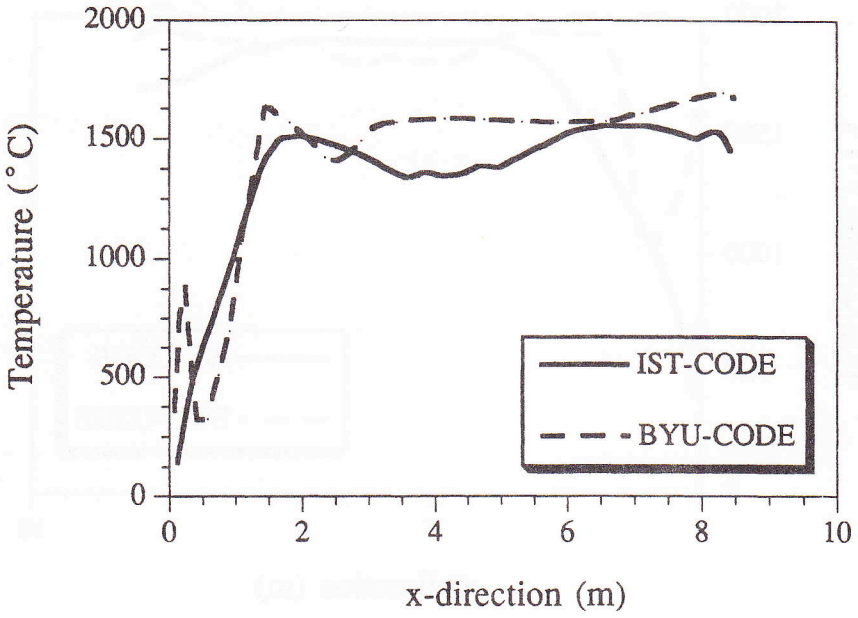

FIGURE 12 Predicted temperatures along the axis of burner 1.

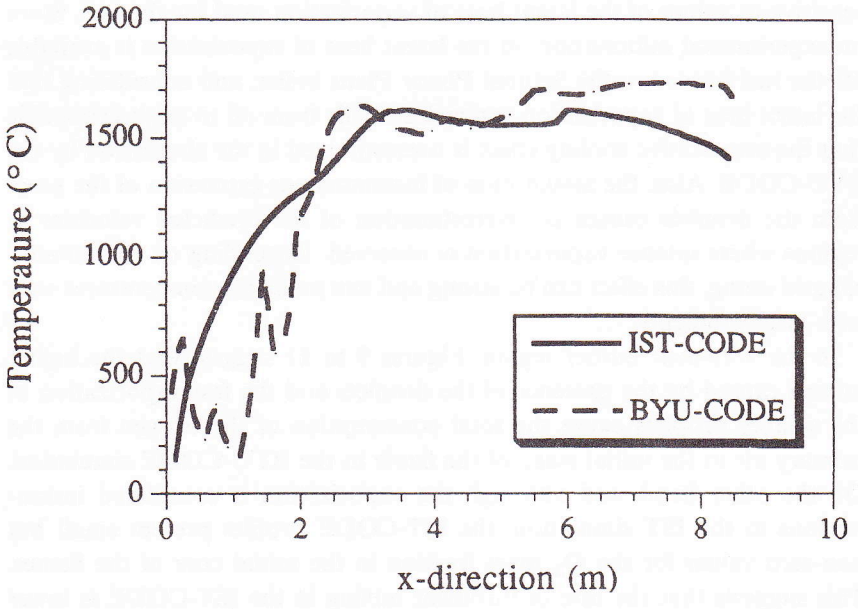

FIGURE 13 Predicted temperatures along the axis of burner 3.

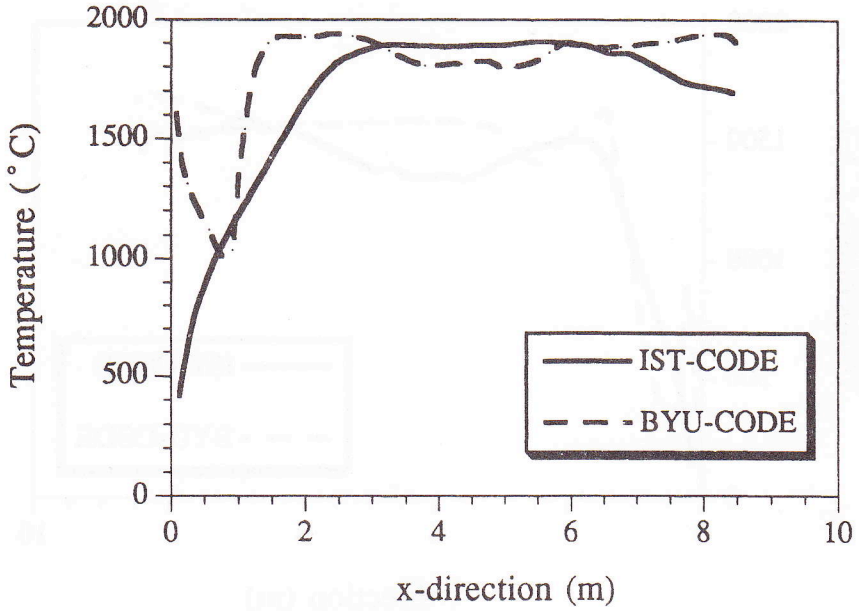

FIGURE 14 Predicted temperatures along the axis of burner 6.

sensitive to values of the latent heat of vaporization used for the fuel. Since no experimental information on the latent heat of vaporization is available for the fuel burned in the Setúbal Power Plant boiler, and considering that the latent heat of vaporization varies drastically from oil to oil, it is possible that the evaporative cooling effect is overestimated in the simulation by the BYU-CODE. Also, the assumption of instantaneous expansion of the gases from the droplets causes an overestimation of the predicted velocities in regions where intense vaporization is observed. Depending on the numerical grid sizing, this effect can be strong and can make the temperatures vary with large gradients.

In the very-near burner region, Figures 9 to 11 suggest that the higher mixing caused by the presence of the droplets and the fast vaporization of the smaller droplets cause the total consumption of the oxygen from the primary air in the initial stage of the flame in the BYU-CODE simulation. On the other hand, and although the vaporization is considered instantaneous in the IST simulation, the IST-CODE profiles present small but non-zero values for the O_2 mass fraction in the initial core of the flames. This suggests that the rate of turbulent mixing in the IST-CODE is lower than it is in the BYU-CODE. The explanation for the different mixing rates

relates to the consideration of the vaporizing droplets. Because the overall volumetric loading of this flow (the ratio of fuel volumetric flow rate to air volumetric flow rate) is lower than 10^{-4}, turbulence modulation from the droplets was not considered. Therefore, the sources from the droplets do not modify directly the gas turbulence field, but only through the introduction of momentum sources (or sinks) to the gas field. These sources (or sinks) generate higher velocity gradients, which cause higher mixing rates.

Figures 15 to 17 show the axial velocity for burners 1, 3, and 6, respectively. As discussed before, the effect of the vaporization of the droplets has a substantial influence on the velocities for the near burner region in the BYU-CODE simulation. For the region beyond $x = 4$ m, where almost all the droplets have vaporized, the simulations performed by both codes agree quite well.

It is also important to emphasize that, because of the differences in modeling the oil vaporization, the boundary conditions in both codes are forced to be different, especially for the inlet cells of fuel oil in the IST-CODE, and the central primary air cells in the BYU-CODE (see Fig. 2). In the IST-CODE, the sharp change in density from the fuel oil cell (liquid) and the first cell in the calculation domain (vapor) results in a lower initial

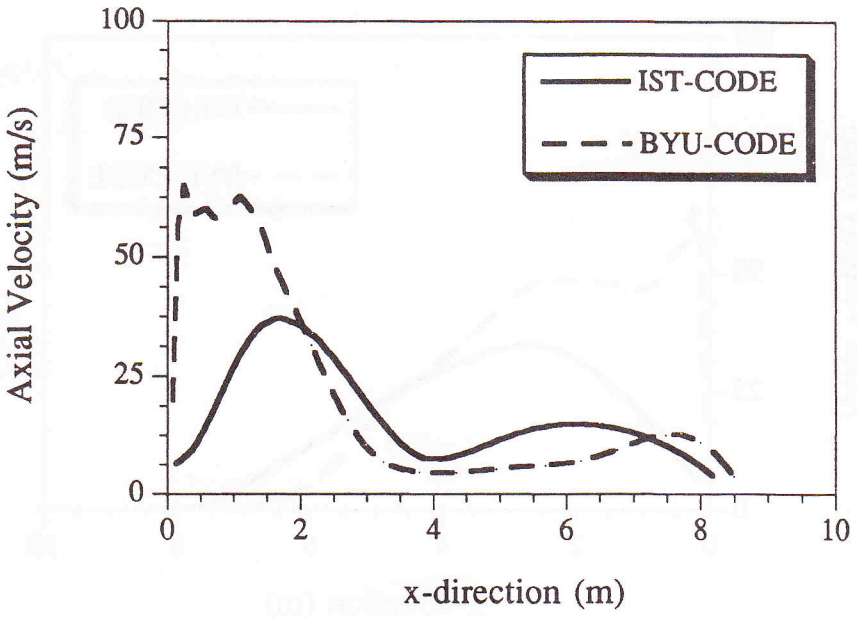

FIGURE 15 Predicted axial velocities along the axis of burner 1.

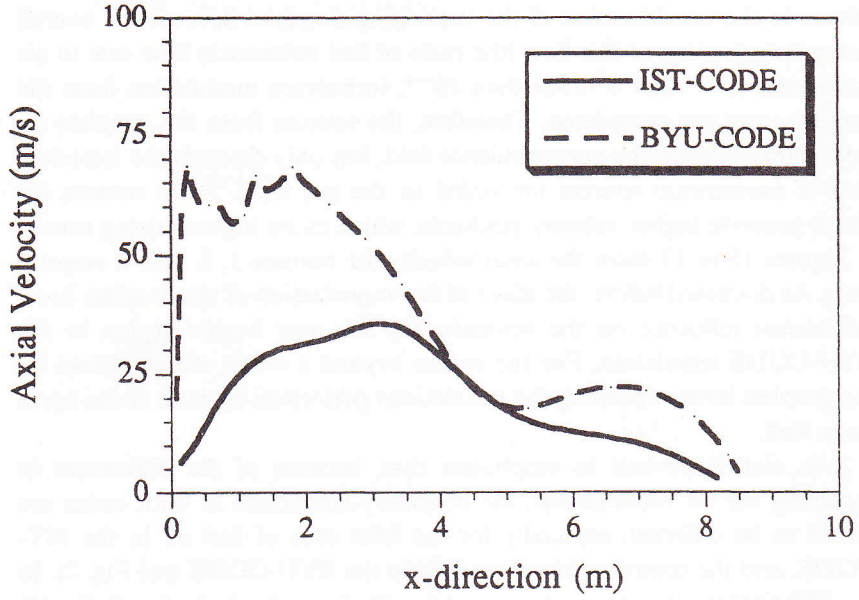

FIGURE 16 Predicted axial velocities along the axis of burner 3.

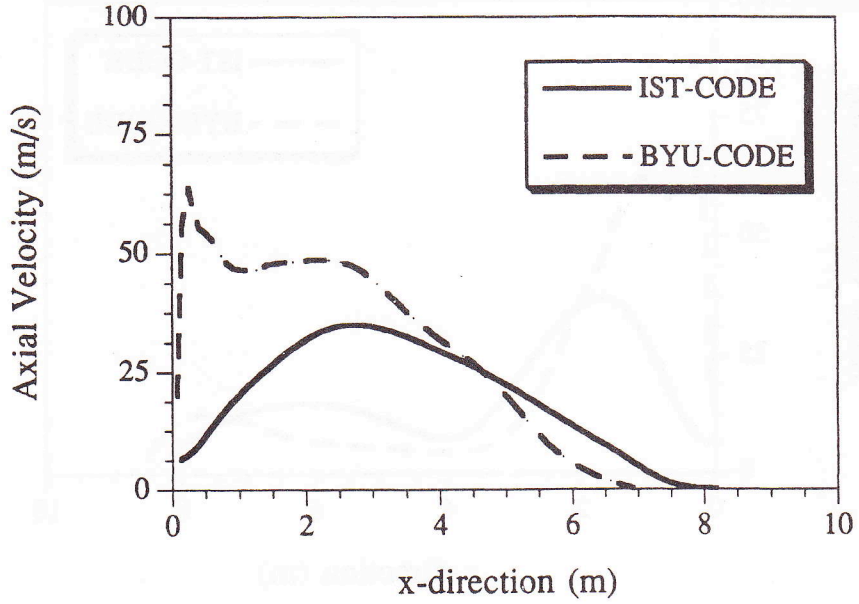

FIGURE 17 Predicted axial velocities along the axis of burner 6.

velocity for the core of the flame. In the BYU-CODE, the droplets were assumed to enter the calculation domain with 90% of the gas velocity of the primary air. These differences in boundary conditions, plus the effect of the vaporizing droplets, result in the major differences found in the very-near burner region.

5. CONCLUSIONS

This paper compares the ability of two comprehensive numerical codes to predict temperature and species concentrations in the radiant section of a large-scale, oil-fired boiler. Although employing different techniques for solving the transport equations and for modeling radiation heat exchange, droplet vaporization, and optical properties of the participating medium, the results from both codes are very satisfactory.

This work corroborates studies which indicate that the current numerical models are capable of predicting temperature and species concentrations within engineering accuracy for industrial-scale, oil-fueled furnaces. The use of simplified kinetics for the combustion reactions showed minor effects in the overall result of the simulations, indicating that a simple chemistry allied with a more refined numerical solution of the near-burner region (such as the use of a spray model combined with local refinement techniques) is more relevant for the numerical results than the incorporation of several-step-reaction combustion models for the entire furnace.

The numerical simulation of the near-burner region might be improved by the local use of more complex kinetics and by the use of a second-moment closure for the turbulence modeling. However, this would be only worthwhile if an accurate discretization of the burners geometry were implemented and if the inlet boundary conditions were known accurately. Nevertheless, the close agreement between predictions and measurements reported in this work suggests that the improvement on the predictions beyond the near-burner region would not be strongly affected.

From this and previous related works (Carvalho *et al.*, 1994; Coimbra *et al.*, 1994; Hill and Smoot; 1993) we conclude that the uncertainties in the characterization of the burner aerodynamics are the major contributors to the deviations from the experimental data observed in the simulations. This indicates that further developments in this area will depend on better characterization of the operating conditions of the boilers. Therefore, it is necessary to have detailed and spatially resolved measurements of the burner aerodynamics under real operating conditions.

Acknowledgements

One of the authors (CFMC) gratefully acknowledges the financial support given by the Brazilian government through a grant from CAPES (Coordenadoria de Aperfeicoamento de Pessoal de Nível Superior). The part of this work performed at BYU was sponsored by ACERC (Advanced Combustion Engineering Research Center) and by ESEERCO (Empire State Electric Energy Research Corporation). Funds for ACERC are received from the National Science Foundation, The State of Utah, 32 industrial participants, and the U.S. Department of Energy. The work performed at Instituto Superior Técnico was sponsored by the European Commission within the framework of the ESPRIT II program. The authors are indebted to Electricidade de Portugal for the cooperation in providing data and access to the boiler.

NOMENCLATURE

B	Transfer Number
C	Empirical Convection Factor
C_D	Drag Coeffient
C_p	Heat Capacity at Constant Pressure
D	Diameter
F	Flux
g	Gravity Acceleration
k	Conductivity or Turbulent Kinetic Energy
L	Latent Heat of Vaporization
m	Mass
Nu	Nusselt Number
Pr	Prandtl Number
Re	Reynolds Number
S	Source Term
T	Temperature
u	Velocity Component
V	Velocity

Greek Symbols

ε	Rate of Dissipation of Turbulent Kinetic Energy
ϕ	Transported Property
Γ	Diffusion Coefficient

μ Dynamic Viscosity
ρ Specific Mass
τ Droplet Relaxation Time

Subscripts
d Droplet
i i-direction
g Gas

Superscripts
c Coarse zone
i i-th Time Step
f Fine zone

References

Abraham, K. U. and Rajaram, S. (1983) Measurements of Furnace Heat Transfer Performance on a Corner-Fired, Pulverized Coal Boiler, *Journal of the Institute of Fuel*, pp. 217–224.

Anson, D., Godridge, A. M. and Hammond, E. G. (1974) Comparison of the Calculated and Measured Heat Transfer Distribution in an Oil-Fired, Water-Tube Boiler, *Journal of the Institute of Fuel*, pp. 83–90.

Aoki, H., Tanno, S., Miura, T. and Ohnishi, S. (1992) Three-Dimensional Spray Combustion Simulation in a Practical Boiler, *JSME International Journal, Series II*, **35** (3), pp. 428–434.

Barlow, S. M. (1982) Laser-Doppler Anemometry Measurements in a Large Gas-Fired Furnace, *Proc. Int. Symp. on Appl. LDA to Fluid Mechanics*, Lisbon, Portugal.

Barreiros, A., Carvalho, M. G., Costa, M. and Lockwood, F. C. (1993) Prediction of the Near Burner Region and Measurements of NO_x and Particulate Emissions in Heavy Fuel Oil Spray Flames, *Combustion and Flame*, **92**, pp. 231–240.

Benesh, W. and Kremer, H. (1984) Mathematical Modelling of Fluid Flow and Mixing in Tangentially Fired Furnaces, *Proc. 20th Symp. (Int.) on Combustion, The Combustion Institute*, pp. 549–557.

Bonin, M. P. and Queiroz, M. (1991) Local Particle Velocity, Size and Concentration Measurements in an Industrial Scale Pulverized Coal Fired Boiler, *Combustion and Flame*, **85**, pp. 121–133.

Boyd, R. K. and Kent, J. H. (1986) Three-Dimensional Furnace Computer Modelling, *Proc. 21th Symp. (Int.) on Combustion, The Combustion Institute*, pp. 265–274.

Butler, B. W. and Webb, B. W. (1991) Local Temperature and Wall Radiant Heat Flux Measurements in an Industrial-Scale, Coal-Fired Boiler, *Fuel*, **70**, pp. 1457–1464.

Carvalho, M. G. and Coelho, P. J. (1990) Numerical Prediction of an Oil-Fired Water Tube Boiler, *Engineering Computations*, **7**(3), pp. 227–234.

Carvalho, M. G., Coelho, P. J., Moreira, A. L. N., Silva, A. M. C. and Silva, T. F. (1994) Comparison of Measurements and Predictions of Wall Heat Flux and Gas Composition in an Oil-Fired Utility Boiler, *Proc. 25th Symp. (Int.) on Combustion, The Combustion Institute*, pp. 227–234.

Cassiano, J., Heitor, M. V., Moreira, A. L. N. and Silva, T. F. (1994) Temperature, Species and Heat Transfer Characteristics of a 250 MWe Utility Boiler, *Combustion Science and Technology*, **98**(1–3), pp. 199–215.

Chen, J. Y., Mann, A. P. and Kent, J. H. (1992) Computational Modelling of Pulverised Fuel Burnout in Tangentially Fired Furnaces, *Proc. 24th Symp. (Int.) on Combustion, The Combustion Institute*, pp. 1381–1389.

Coelho, P. J. and Carvalho, M. G. (1993) Application of a Domain Decomposition Technique to the Mathematical Modelling of a Utility Boiler, *International Journal for Numerical Methods in Engineering*, **36**, pp. 3401–3419.

Coimbra, C. F. M. and Queiroz, M. (1994) CFD Modelling of Multiphase Oil Droplet Combustion in a 20 MWe Industrial Boiler, *Proceedings of the 5th Brazilian Thermal Science Meeting-V ENCIT*, São Paulo, pp. 379–382.

Coimbra, C. F. M., Azevedo, J. L. T. and Carvalho, M. G. (1994) 3-D Numerical Model for Predicting NOx Emissions from an Industrial Pulverized Coal Combustor, *Fuel*, **73** (7), pp. 1128–1134.

Costa, M., Costen, P., Lockwood, F. C. and Mahmud, T. (1990) Detailed Measurements in and Modelling of an Industry-Type Pulverised-Coal Flame, *Proc. 23th Symp. (Int.) on Combustion, The Combustion Institute*, pp. 973–980.

De Michelle, G., Ghiribelli, L., Pasini, S. and Tozzi, A. (1989) A 3-D Code for Predicting Radiative and Convective Heat Transfer in Boilers, *National Heat Transfer Conference, HTD* **106**, *Heat Transfer Phenomena in Radiation, Combustion and Fires*, pp. 275–286.

Denison, M. K. and Webb, B. W. (1993) A Spectral Line-Based Weighted-Sum-of-Gray-Gases Model for Arbitrary RTE Solvers, *Journal of Heat Transfer*, **115**, pp. 1004–1012.

Fiveland, W. A. (1987) A Discrete Ordinates Method for Radiation Transfer, *American Society of Mechanical Engineers--Heat Transfer Division*, pp. 9–19.

Fiveland, W. A. and Wessel, R. A. (1988) Numerical Model for Predicting Performance of Three-Dimensional Pulverized-Fuel Fired Furnaces, *ASME Trans. J. Eng. Gas Turbines Power*, pp. 117–126.

Gillis, P. A. and Smith, P. J. (1990) An Evaluation of Three-Dimensional Computational Combustion and Fluid-Dynamics for Industrial Furnaces Geometries, *Proc. 23th Symp. (Int.) on Combustion, The Combustion Institute*, pp. 981–991.

Gopinath, R. and Ganesan, V. (1994) Numerical Predictions of Temperature and Species Concentration in Three-Dimensional Reacting Flows - a New Approach, *Journal of the Institute of Energy*, **67**, pp. 10–18.

Hanjalic, K. and Sijercic, M. (1994) Application of Computer Simulation in a Design Study of a New Concept of Pulverized Coal Gasification - Part I, *Combustion Science and Technology*, **97**, pp. 331–350.

Heitor, M. V., Moreira, A. L. N., Silva, A. M. C. and Silva, T. F. (1994) Experimental Analysis of the In-Furnace Processes in a 250 MWe Oil-Fired Utility Boiler, *presented at the 10th International Heat Transfer Conference*, August, 14–18, Brighton, England.

Hill, S. C. and Smoot, L. D. (1993) A Comprehensive Three-Dimensional Model for Simulation of Combustion Systems: PCGC-3, *Energy and Fuels*, **7**, pp. 874-883.

Khan, I. M. and Greeves, G. A. (1974) A Method for Calculating the Formation and Combustion of Soot in Diesel Engines, in *Heat Transfer in Flames*, Afgan, N. H. and Beer, J. M. (Ed.), Scripta Book Co., pp. 391–402.

Lockwood, F. C. and Shah, N. G. (1980) A New Radiation Solution Method for Incorporation in General Combustion Prediction Procedures, *Proc. 18th Symp. (Int.) on Combustion, The Combustion Institute*, pp. 1919–1925.

Lockwood, F. C., Papadopoulos, C. and Abbas, A. S. (1988) Prediction of a Corner-Fired Power Station Combustor, *Combustion Science and Technology*, **58**, pp. 43–57.

Lockwood, F. C., Salooja, A. P. and Syed, S. A. (1980) A Prediction Method for Coal-Fired Furnaces, *Combustion and Flame*, **38**, pp. 1–15.

Magnussen, B. F. and Hjertager, B. H. (1977) On Mathematical Modelling of Turbulent Combustion, with Special Emphasis on Soot Formation and Combustion, *Proc. 16th Symp. (Int.) on Combustion, The Combustion Institute*, pp. 549–557.

Mann, A. P. and Kent, J. H. (1994) A Computational Study of Heterogeneous Char Reactions in a Full-Scale Furnace, *Combustion and Flame*, **99**, pp. 147–156.

Queiroz, M., Bonin, M. P., Shirolkar, J. S. and Dawson, R. W. (1993) Experimentally Determined Particle Number Density Statistics in an Industrial-Scale, Pulverized-Coal-Fired Boiler, *Energy and Fuels*, **7**, pp. 842–851.

Rizvi, S. M. A. (1985) Prediction of Flow, Combustion, and Heat Transfer in Pulverized Coal Flames, Ph.D. Dissertation, Imperial College of London, University of London.

Robinson, G. F. (1985) A Three-Dimensional Analytical Model of a Large Tangentially-Fired Furnace, *Journal of the Institute of Energy*, **37**, pp. 116–150.

Sakai, M., Tokuda, K., Ide, Y., Nakashima, F., Asayama, H. and Aiki, H. (1982) Development of Three-Dimensional Numerical Analysis Method of Boiler Furnace Characteristics - Part II: Combustion and Heat Transfer Analysis, *Technical Review*, pp. 24–35.

Shida, H., Karagasaki, M., Adachi, T., Kumimoto, T., Hisatome, M. and Kobayashi, I. (1982) Development of Three-Dimensional Numerical Analysis Method of Boiler Furnace Characteristics - Part I: Flow Analysis, *Technical Review*, pp. 18–23.

Sijercic, M. and Hanjalic, K. (1994) Application of Computer Simulation in a Design Study of a New Concept of Pulverized Coal Gasification - Part II, *Combustion Science and Technology*, **97**, pp. 351–374.

Smoot, L. D. (1981) Pulverized Coal Diffusion Flames: A Perspective Through Modeling, *Proc. 18th Symp. (Int.) on Combustion, The Combustion Institute*, pp. 1185–1202.

Truelove, J. S. (1976) A Mixed Grey Gas Model for Flame Radiation, *AERE Report HL76-3448-KE.*

Truelove, J. S. (1986) Prediction of the Near-Burner Flow and Combustion in Swirling Pulverized-Coal Flames, *Proc. 21st Symp. (Int.) on Combustion, The Combustion Institute*, pp. 275–284.

Truelove, J. S., Williams, R. G. (1988) Coal Combustion Models for Flame Scaling, *Proc. 22nd Symp. (Int.) on Combustion, The Combustion Institute*, pp. 155–164.

Xu, X. -C. (1981) Mathematical Modelling of Three-Dimensional Heat Transfer from the Flame in Combustion Chambers, *Proc. 18th Symp. (Int.) on Combustion, The Combustion Institute*, pp. 1919–1925.